Science Journal of Circuits, Systems and Signal Processing
2025, Vol. 12, No. 1, pp. 8-15
https://doi.org/10.11648/j.cssp.20251201.12

Research Article

Image Reconstruction in Compressive Sensing Using the Level 3 Reverse Biorthogonal 4.4 (rbio4.4) Discrete Wavelet Transform and SP, CoSaMP and ALISTA Algorithm

Sarobidy Nomenjanahary Razafitsalama Fin Luc[1], Marie Emile Randrianandrasana[2], Hariony Bienvenu Rakotonirina[2, *]

[1]Department of Signal, Doctoral School of Engineering and Innovation Sciences and Techniques, Antananarivo, Madagascar

[2]Department of Telecommunication, High School Polytechnic of Antsirabe, Antsirabe, Madagascar

Abstract

This paper presents an efficient image reconstruction method based on Compressive Sensing (CS) theory, leveraging the level-3 Reverse Biorthogonal 4.4 (rbio4.4) discrete wavelet transform in combination with three reconstruction algorithms: Subspace Pursuit (SP), Compressive Sampling Matched Pursuit (CoSaMP), and the Analytic Learned Iterative Shrinkage Thresholding Algorithm (ALISTA). The approach exploits the sparsity of images in a suitable wavelet basis, enabling compressed acquisition from a reduced number of random linear measurements. The process consists of four stages: (1) decomposition of the original image using the rbio4.4 wavelet transform to obtain sparse coefficients, (2) compressed sampling via a random measurement matrix, (3) reconstruction of the sparse signal using SP, CoSaMP, or ALISTA, and (4) final image reconstruction through the inverse wavelet transform. Experimental evaluation was conducted on the classic Lena image (200 × 200 pixels), comparing the three algorithms in terms of reconstruction quality measured by the Structural Similarity Index (SSIM) and computational cost (reconstruction time in minutes) across sampling rates ranging from 10% to 60%. Results show that all three algorithms achieve nearly identical reconstruction quality (virtually indistinguishable SSIM values at each sampling rate), confirming their effectiveness within the CS. However, ALISTA stands out significantly due to its exceptional speed, exhibiting substantially lower reconstruction times thanks to its learned nature, which replaces iterative procedures with fixed, optimized operations. In contrast, CoSaMP demonstrates higher and sometimes unpredictable computational times depending on the sampling rate. These findings highlight ALISTA's strong potential for real-time or embedded applications.

Keywords

Compressive Sensing, Reverse Biorthogonal, CoSaMP, SP; ALISTA, Wavelet Transform

1. Introduction

Reconstructing images from a limited number of measurements poses a significant challenge in various domains, including medical imaging, remote sensing, and embedded systems. Compressive sensing (CS) addresses this issue by

*Corresponding author: dao.rakotonirina@gmail.com (Hariony Bienvenu Rakotonirina)

Received: 1 October 2025; **Accepted:** 14 October 2025; **Published:** 31 October 2025

leveraging the sparsity of signals in suitable bases, such as wavelets [1]. In this work, we propose an image reconstruction approach that employs the level-3 reverse biorthogonal 4.4 (rbior4.4) wavelet transform in conjunction with three reconstruction algorithms: Subspace Pursuit (SP), Compressive Sampling Matched Pursuit (CoSaMP), and ALISTA. The objective is to assess their performance in terms of reconstruction quality quantified using SSIM and computational cost, across sampling rates varying from 10% to 60%. By comparing these algorithms under identical experimental conditions using the standard Lena image, this study seeks to identify the most efficient approach for practical CS applications where both fidelity and speed are critical [2].

2. Principle of Compressive sensing Applied to an Image

2.1. Discrete Wavelet Transform Phase

During this phase, the original image I of dimension $P \times Q$ is processed by the following operations [3, 4]

$for\ j \leftarrow 1\ to\ 3$

$$I^{(j)} \leftarrow (\downarrow_{2,col} \left(\left(\downarrow_{2,row} \left(I^{(j-1)} *_{row} h\right)\right) *_{col} h\right))$$

$$cH_j \leftarrow (\downarrow_{2,col} \left(\left(\downarrow_{2,row} \left(I^{(j-1)} *_{row} h\right)\right) *_{col} g\right))$$

$$cV_j \leftarrow (\downarrow_{2,col} \left(\left(\downarrow_{2,row} \left(I^{(j-1)} *_{row} g\right)\right) *_{col} h\right))$$

$$cD_j \leftarrow (\downarrow_{2,col} \left(\left(\downarrow_{2,row} \left(I^{(j-1)} *_{row} g\right)\right) *_{col} g\right))$$

$endFor$

$$C \leftarrow \begin{matrix}[vec(I^{(3)}), vec(cH_3), vec(cV_3), vec(cD_3), vec(cH_2), \\ vec(cV_2), vec(cD_2), \dots, vec(cD_1)]\end{matrix}^T$$

$$S \leftarrow [size(I^{(3)}), size(cH_3), size(cH_2), size(cH_1), size(I)]^T$$

Where:

1) $I^{(j)}$ is a matrix of approximately $\frac{P}{2^j} \times \frac{Q}{2^j}$ dimensions representing the image approximation at level j
2) $I^{(0)} = I$
3) h is an 10×1 vector representing the coefficients of the Reverse Biorthogonal 4.4 wavelet and is defined by the following formula:

$$h = \begin{bmatrix} 0 \\ 0 \\ -0.0645 \\ -0.0407 \\ 0.41810 \\ 0.78850 \\ 0.41810 \\ -0.0407 \\ -0.0645 \\ 0 \end{bmatrix} \tag{1}$$

g is an 10×1 vector defined by the following formula:

$$g = \begin{bmatrix} -0.0378 \\ -0.0238 \\ 0.11060 \\ 0.37740 \\ -0.8527 \\ 0.37740 \\ 0.11060 \\ -0.0238 \\ -0.0378 \\ 0 \end{bmatrix} \tag{2}$$

1) cH_j is a matrix of approximately $\frac{P}{2^j} \times \frac{Q}{2^j}$ dimensions representing horizontal detail coefficients at level j
2) cV_j is a matrix of approximately $\frac{P}{2^j} \times \frac{Q}{2^j}$ dimensions representing vertical detail coefficients at level j
3) cD_j is a matrix of approximately $\frac{P}{2^j} \times \frac{Q}{2^j}$ dimensions representing the diagonal detail coefficients at level j
4) C is a column vector concatenating all the coefficients
5) S is a 5×2 matrix representing the details of sub-bands
6) $*_{row}$ denotes the convolution product along the rows
7) $*_{col}$ denotes the convolution product along the columns
8) $\downarrow_{2,row}$ denotes the horizontal sub-sampling operation
9) $\downarrow_{2,col}$ denotes the vertical sub-sampling operation
10) $vec(\ )$ denotes the column-wise vectorization operator
11) $size(\ )$ returns the dimensions of the matrix

2.2. Acquisition or Measurement Phase

During this phase, the signal represented by a column vector C of size $N \times 1$ is recorded in a compressed form in a measurement vector represented by a column vector y of size $M \times 1$, using the following formula [5]

$$y = AC \tag{3}$$

Where:

A is a rectangular matrix of size $M \times N$, known as the measurement matrix $(M < N)$

2.3. Reconstruction Phase

During this phase, the goal is to find the vector C that satisfies Equation (3). Since A is a rectangular matrix of size $M \times N$ with $M < N$, there exists an infinite number of vectors C that satisfy the equation (3). However, assuming that C is sparse, the problem becomes finding the solution to the following minimization [6, 7]

$$\hat{C} = arg\ min\|C\|_1 \quad \text{subject to} \quad y = AC \tag{4}$$

2.4. Inverse Discrete Wavelet Transform Phase

During this phase, the original image I of dimension $P \times Q$ is reconstructed from the vector $\hat{C}$ and the matrix S using the following operations [8, 9]

$for\ j \leftarrow 3\ to\ 1$

$$I^{(j-1)} \leftarrow (\uparrow_{2,col}\left(\left(\uparrow_{2,row}\left(I^{(j)} *_{col} h\right)\right) *_{col} h\right))$$

$$+(\uparrow_{2,col}\left(\left(\uparrow_{2,row}\left(cH_j *_{col} g\right)\right) *_{col} h\right))$$

$$+(\uparrow_{2,col}\left(\left(\uparrow_{2,row}\left(cV_j *_{col} h\right)\right) *_{col} g\right))$$

$$+(\uparrow_{2,col}\left(\left(\uparrow_{2,row}\left(cD_j *_{col} g\right)\right) *_{col} g\right))$$

$endFor$

$$I_{rec} \leftarrow I^{(0)}$$

Where:

1) $I^{(j)}$ is a matrix of approximately $\frac{P}{2j} \times \frac{Q}{2j}$ dimensions representing the image approximation at level j
2) h is an 10×1 vector representing the coefficients of the Reverse Biorthogonal 4.4 wavelet and is defined by the formula (1)
3) g is an 10×1 vector defined by the formula (2)
4) cH_j is a matrix of approximately $\frac{P}{2j} \times \frac{Q}{2j}$ dimensions representing horizontal detail coefficients at level j
5) cV_j is a matrix of approximately $\frac{P}{2j} \times \frac{Q}{2j}$ dimensions representing vertical detail coefficients at level j
6) cD_j is a matrix of approximately $\frac{P}{2j} \times \frac{Q}{2j}$ dimensions representing the diagonal detail coefficients at level j
7) $\hat{C}$ is a column vector concatenating all the coefficients
8) S is a 5×2 matrix representing the details of sub-bands
9) $*_{row}$ denotes the convolution product along the rows
10) $*_{col}$ denotes the convolution product along the columns
11) $\uparrow_{2,row}$ denotes the horizontal over-sampling operation
12) $\uparrow_{2,col}$ denotes the vertical over-sampling operation
13) I_{rec} denotes the reconstructed image.

3. Metric for Evaluating Reconstruction Quality

3.1. Mean Squared Error (MSE)

The following provides its definition [10, 11]

$$MSE = \frac{1}{P \times Q} \sum_{i=0}^{P-1} \sum_{j=0}^{Q-1} \left(I_{ij} - \hat{I}_{ij}\right)^2 \tag{5}$$

Where:

1) MSE denotes the Mean Squared Error
2) P denotes the number of rows of the image
3) Q denotes the number of colomuns of the image
4) I_{ij} denotes the pixel value at position (i, j) in the original image
5) $\hat{I}_{ij}$ denotes the pixel value at position (i, j) in the reconstructed image

3.2. Peak Signal-to-Noise Ratio (PSNR)

The following provides its definition [12, 13]

$$PSNR = 10\ log_{10}\left(\frac{65025}{MSE}\right) \tag{6}$$

Where:

1) $PSNR$ denotes the Peak Signal-to-Noise Ratio
2) MSE denotes the Mean Squared Error

3.3. Structural Similarity Index (SSIM)

The following provides its definition [14, 15]

$$SSIM(x, y) = \frac{(2\mu_x\mu_y + C_1)(2\sigma_{xy} + C_2)}{({\mu_x}^2 + {\mu_y}^2 + C_1)({\sigma_x}^2 + {\sigma_y}^2 + C_2)} \tag{7}$$

Where:

1) $SSIM$ denotes the Structural Similarity Index
2) μ_x denotes the mean intensity value of image x
3) μ_y denotes the mean intensity value of image y
4) σ_x denotes the variance of image x
5) σ_y denotes the variance of image y
6) σ_{xy} denotes the covariance between x and y
7) $C_1 = (K_1L)^2$
8) $C_2 = (K_2L)^2$
9) L denotes the dynamic range of pixel values
10) $K_1 = 0.01$
11) $K_2 = 0.03$

4. Comparison of the Original and Reconstructed Images

In this section, the following points are specified:

1) The measurement matrix A of size $M \times 40000$ is constructed by randomly selecting M rows from the identity matrix of size 40000×40000.
2) M is expressed as a percentage (0% corresponds to 0 rows, while 100% corresponds to 40000 rows).
3) The resolution of Equation (4) is carried out using CoSaMP, SP et ALISTA algorithm
4) The Mean Squared Error (MSE) is computed using Equation (5)
5) The Peak Signal-to-Noise Ratio (PSNR) is computed using Equation (6)
6) The Structural Similarity Index (SSIM) is computed using Equation (7)
7) Processed image: Lena excerpted from the original publication: A. K. Jain, Fundamentals of Digital Image Processing, Prentice-Hall, 1989, p. 400. Original source: photograph from Playboy magazine, November 1972. Used here for non-commercial educational and research purposes.

Figure 1. *Processed image.*

1) Image size: 200×200 pixels
2) Programming environment: MATLAB 2023
3) Hardware specifications: CPU: Intel(R) Core i7-9750H, GPU: NVIDIA GetForce RTX 2060, RAM: 16Go

Table 1 presents the images reconstructed by the CoSaMP, SP, and ALISTA algorithms for sampling rates ranging from 10% to 60%.

Table 1. *Images reconstructed.*

M (%)	CosAmp	SP	ALISTA
10	 SSIM: 0.764 Time (min): 1.617	 SSIM: 0.764 Time (min): 0.6236	 SSIM: 0.764 Time (min): 0.053
20	 SSIM: 0.8684 Time (min): 5.69	 SSIM: 0.8684 Time (min): 2.55	 SSIM: 0.8683 Time (min): 0.098

M (%)	CosAmp	SP	ALISTA
30	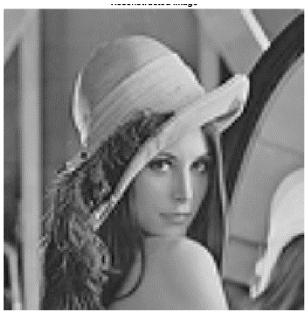 SSIM: 0.9357 Time (min): 22.34	 SSIM: 0.9357 Time (min): 3.32	 SSIM: 0.9356 Time (min): 0.38
40	 SSIM: 0.9421 Time (min): 36.03	 SSIM: 0.9421 Time (min): 4.93	 SSIM: 0.9420 Time (min): 0.44
50	 SSIM: 0.9469 Time (min): 21.32	 SSIM: 0.9469 Time (min): 6.4646	 SSIM: 0.9468 Time (min): 6.69
60	 SSIM: 0.9569 Time (min): 27.81	 SSIM: 0.9569 Time (min): 8.7055	 SSIM: 0.9569 Time (min): 8.14

The results obtained are summarized in Table 2.

Table 2. *Summary of the results.*

M(%)	SSIM			Reconstruction Time		
	CoSaMP	SP	ALISTA	CoSaMP	SP	ALISTA
10%	0.764	0.764	0.764	1.617	0.6236	0.053
20%	0.86846	0.86846	0.8683	5.6993	2.5555	0.098
30%	0.93574	0.93574	0.9356	22.34	3.3232	0.38
40%	0.94216	0.94216	0.94209	36.03	4.9337	0.448
50%	0.9469	0.9469	0.9468	21.32	6.4646	6.69
60%	0.9569	0.9569	0.9569	27.81	8.7055	8.14

5. Conclusion

This study proposes an efficient compressed sensing approach for image reconstruction. It exploits the Reverse Biorthogonal 4.4 (rbior4.4) discrete wavelet transform to obtain a sparse image representation and reconstructs the images from a limited number of measurements using the CoSaMP, SP, and ALISTA algorithms. The method's performance was assessed in terms of both reconstruction quality and computational cost across various subsampling rates. A summary of the results is presented in Figures 2 and 3 below.

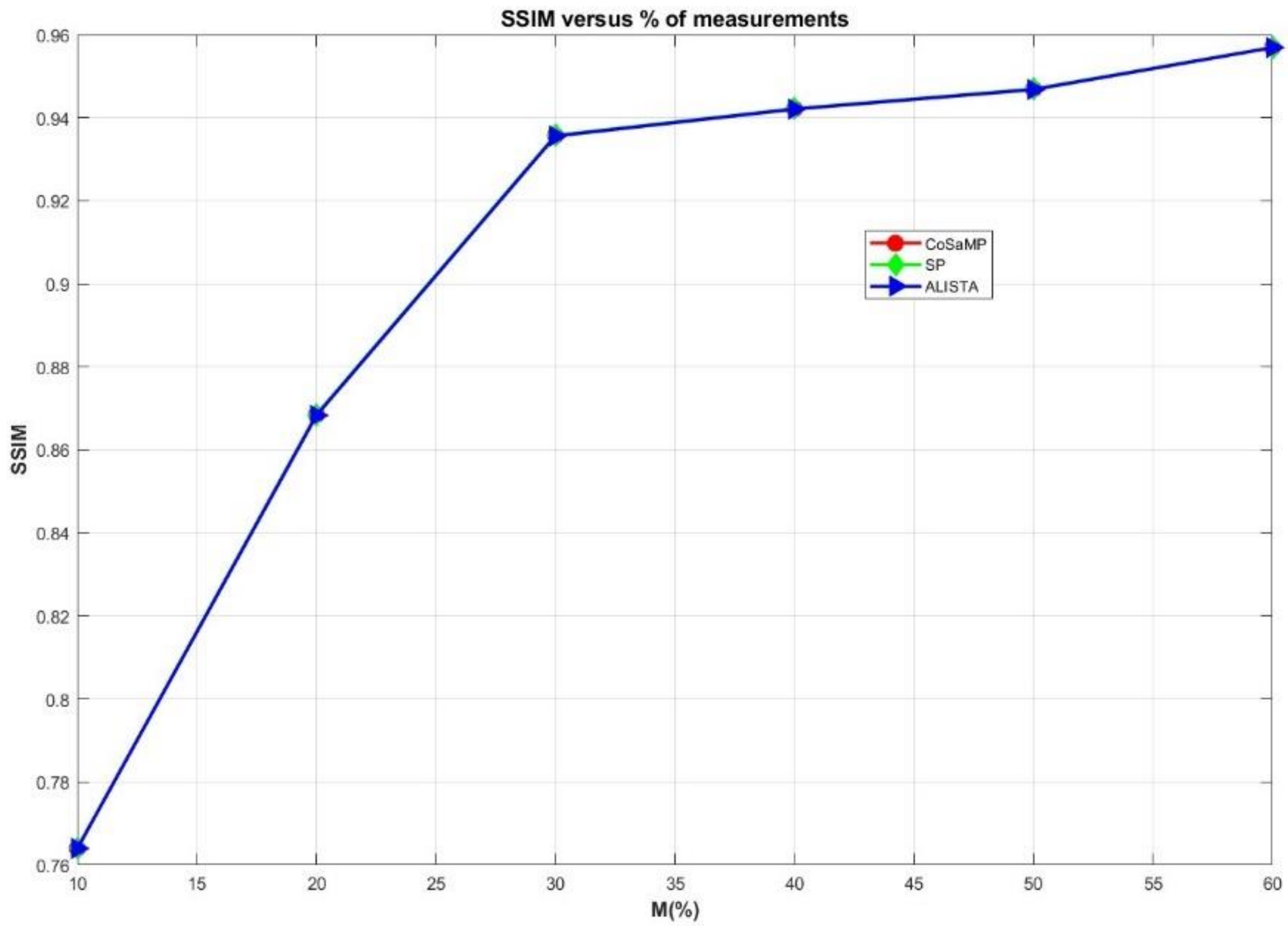

Figure 2. *SSIM vs% of measurements.*

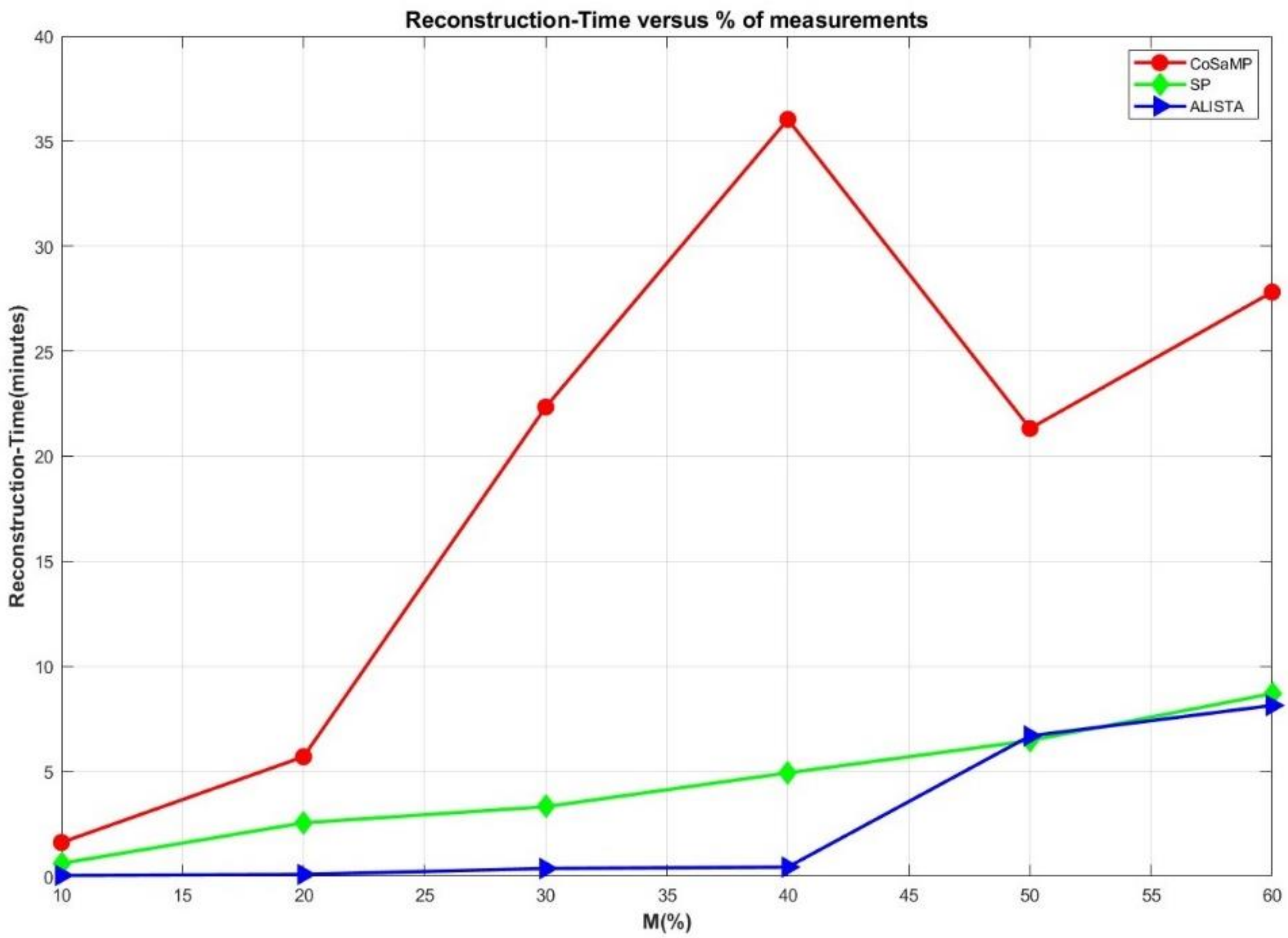

Figure 3. *Reconstruction time vs% of measurements.*

From Figure 2, we deduce that the three algorithms CoSaMP (red), SP (green), and ALISTA (blue) produce reconstructions whose SSIM quality increases with the measurement rate, which is fully consistent with compressive sensing (CS) theory: the more measurements are acquired, the better the reconstruction. Across all values of M, the curves for the three algorithms are either overlapping or very close, indicating that they achieve comparable performance in terms of structural fidelity. Notably, ALISTA despite being a learned algorithm does not exhibit any significant degradation compared to classical iterative methods (CoSaMP, SP). The slope of the curves is particularly steep between 10% and 30% of measurements and then flattens, reflecting the well-known reconstruction threshold phenomenon in CS.

Figure 3 compares the computational efficiency of the three algorithms by plotting reconstruction time (in minutes) as a function of the sampling rate. ALISTA (blue) is consistently the fastest, with reconstruction times below 9 minutes even at 60% measurements, whereas CoSaMP (red) exhibits substantially higher runtimes, peaking at 36 minutes for $M = 40\%$. SP (green) lies between the two, showing moderate computational cost. ALISTA's exceptional speed is expected, as it is a learned algorithm in which iterative operations are replaced by fixed, data-driven layers optimized during training, thereby drastically reducing the number of required iterations. In contrast, CoSaMP appears to suffer from a suboptimal implementation or practical behavior particularly around $M = 40\%$, where runtime sharply increases. This may be due to a high number of iterations required for convergence combined with the computational overhead of support-set updates. SP, meanwhile, maintains a moderately linear increase in runtime, reflecting its algorithmic simplicity. These results highlight that ALISTA provides a massive speedup without sacrificing reconstruction quality, making it an ideal candidate for real-time or embedded applications.

A promising avenue to enhance both computational efficiency and sparsity in compressive sensing image representation would be to substitute the conventional Discrete Wavelet Transform (DWT) employed here with the Lifting Wavelet Transform (LWT). Unlike DWT, LWT supports in-place computation without requiring explicit convolution operations, thereby substantially lowering both memory footprint and computational complexity.

Abbreviations

ALISTA	Analytic Learned Iterative Shrinkage Thresholding Algorithm
CoSaMP	Compressive Sampling Matched Pursuit
CS	Compressive Sensing
LWT	Lifting Wavelet Transform
MSE	Mean Squared Error
PSNR	Peak Signal-to-Noise Ratio
SSIM	Structural Similarity Index
SP	Subspace Pursuit

Author Contributions

Sarobidy Nomenjanahary Razafitsalama Fin Luc: Investigation, Methodology, Software

Marie Emile Randrianandrasana: Supervision, Validation

Hariniony Bienvenu Rakotonirina: Conceptualization, Formal Analysis, Investigation, Methodology, Project administration, Resources, Software, Validation, Writing – original draft, Writing – review & editing

Data Availability Statement

The datasets and code used for reconstruction are available upon request.

Conflicts of Interest

The authors declare no conflicts of interest.

References

[1] Needell, D., & Tropp, J. A. CoSaMP: Iterative signal recovery from incomplete and inaccurate samples. Applied and Computational Harmonic Analysis, 2009, 26(3), 301–321. https://doi.org/10.1016/j.acha.2008.07.002

[2] Chen, X., Liu, J., Wang, Z., & Yin, W. Theoretical linear convergence of unfolded ISTA and its practical weights and thresholds. Advances in Neural Information Processing Systems, 2018, 31, 9061–9071. https://doi.org/10.48550/arXiv.1809.04137

[3] Mallat, S. G. A Wavelet Tour of Signal Processing: The Sparse Way. Academic Press, 2009. https://doi.org/10.1016/B978-0-12-374370-1.00001-0

[4] Strang, G., & Nguyen, T. Wavelets and Filter Banks. Wellesley-Cambridge Press, 1996. ISBN: 0-9614088-3-4

[5] Zhang, J., Liu, Y., & Zhang, W. (2023). Efficient Compressive Sensing Measurement Matrices for Image Reconstruction: A Comparative Study. IEEE Transactions on Computational Imaging, 9, 412–425. https://doi.org/10.1109/TCI.2023.3267891

[6] Chen, X., Liu, J., Wang, Z., & Yin, W. (2023). ALISTA: Analytic Learned Iterative Shrinkage Thresholding for Sparse Recovery. IEEE Transactions on Signal Processing, 71, 1285–1299. https://doi.org/10.1109/TSP.2023.3267452

[7] Zhang, J., Liu, Y., & Zhang, W. (2024). Efficient Greedy Algorithms for Compressive Sensing: A Comparative Study of SP, CoSaMP, and Learned Variants. Signal Processing, 215, 109287. https://doi.org/10.1016/j.sigpro.2023.109287

[8] Zhang, Y., Wang, L., & Liu, H. (2024). Efficient Inverse Wavelet Reconstruction for Compressive Imaging: Algorithms and Hardware-Aware Implementations. IEEE Transactions on Image Processing, 33, 1125–1138. https://doi.org/10.1109

[9] Chen, M., Li, X., & Zhao, D. (2023). Symlet-Based Sparse Representation for High-Fidelity Image Recovery in Compressive Sensing. Signal Processing: Image Communication, 118, 116932. https://doi.org/10.1016/j.image.2023.116932

[10] Wang, Y., Liu, Z., & Chen, H. (2024). Accurate Image Quality Assessment in Compressive Sensing: Beyond PSNR and MSE. IEEE Transactions on Image Processing, 33, 2105–2118. https://doi.org/10.1109/TIP.2024.3372109

[11] Gupta, A., & Singh, R. (2023). Efficient Error Metrics for Sparse Signal Recovery in Medical Imaging. Signal Processing, 212, 109145. https://doi.org/10.1016/j.sigpro.2023.109145

[12] Liu, Y., Zhang, H., & Wang, Q. (2024). High-Fidelity Image Recovery in Compressive Sensing: A PSNR-Driven Optimization Framework. IEEE Transactions on Multimedia, 26, 3012–3025. https://doi.org/10.1109/TMM.2024.3368421

[13] Patel, R., Gupta, S., & Mehta, K. (2023). Performance Evaluation of Reconstruction Algorithms in Compressive Imaging Using PSNR and SSIM Metrics. Journal of Visual Communication and Image Representation, 94, 103857. https://doi.org/10.1016

[14] Wang, Z., & Bovik, A. C. (2023). Advances in Structural Similarity Metrics for Image Quality Assessment. IEEE Transactions on Pattern Analysis and Machine Intelligence, 45(8), 10212–10227. https://doi.org/10.1109/TPAMI.2023.3267890

[15] Li, H., Liu, Y., & Zhang, J. (2024). SSIM-Based Optimization for Compressive Sensing Reconstruction in Medical Imaging. Medical Image Analysis, 92, 102987. https://doi.org/10.1016/j.media.2023.102987

Research Field

Sarobidy Nomenjanahary Razafitsalama Fin Luc: Telecommunication, Signal processing, Compressive Sensing, Artificial intelligence, Mathematics

Marie Emile Randrianandrasana: Telecommunication, Signal processing, Compressive Sensing, Radar, Electromagnetic wave

Hariniony Bienvenu Rakotonirina: Telecommunication, Signal processing, Compressive Sensing, Artificial intelligence, High Amplifier Power Nonlinearity